High-energy Laser-accelerated Electron Beams for Long-range Interrogation

Nathaniel J. Cunningham, Sudeep Banerjee, Vidya Ramanathan, Nathan Powers, Nate Chandler-Smith, Randy Vane, David Schultz, Sara Pozzi, Shaun Clarke, James Beene, and Donald Umstadter

---

High-energy Laser-accelerated Electron Beams for Long-range Interrogation

Nathaniel J. Cunningham,[1] Sudeep Banerjee,[1] Vidya Ramanathan,[1] Nathan Powers,[1] Nate Chandler-Smith,[1] Randy Vane,[2] David Schultz,[2] Sara Pozzi,[3] Shaun Clarke,[3] James Beene,[2] Donald Umstadter[1]

[1]*Department of Physics & Astronomy, University of Nebraska, Lincoln, NE 68588-0111*
[2]*Physics Division, Oak Ridge National Laboratory, Oak Ridge, TN 37831-6372*
[3]*Department of Nuclear Engineering & Radiological Sciences, University of Michigan, Ann Arbor, MI 48109-2104*

Abstract. We are studying the use of 0.1 - 1.0 GeV laser-accelerated electron beams as active interrogation probes for long-standoff radiography or nuclear activation of concealed special nuclear material. Use of beams in this energy range is largely unexplored, but such beams could provide notable advantages over lower-energy beams and x-rays. High-energy laser-accelerated electrons exhibit large penetration range through air and solids, and low beam divergence for both direct beams and secondary Bremsstrahlung x-rays. We present laboratory measurements of radiography and activation, using the high-power Diocles laser system at the University of Nebraska, as well as MCNP and GEANT Monte Carlo simulation results used to aid experiment design and interpretation.

Keywords: nuclear activation, active interrogation, particle beam radiography, laser wakefield accelerators
PACS: 61.80.Fe, 52.38.Kd, 25.85.Jg, 27.90.+b, 27.50.+e, 25.20.-x

INTRODUCTION

The Diocles laser facility at the University of Nebraska is a 100 TW, 30 fs pulsed Ti:sapphire laser system. When employed as a plasma wakefield accelerator for electrons, Diocles routinely provides electron beams exhibiting high energy (up to 400 MeV), with high beam charge (~0.6 nC), narrow energy width (~10%), and small angular divergence (6mrad full-width half-maximum, FWHM). The laser can be fired at rates up to 10 Hz. The Diocles laser system is compact, with a 200 sq. ft. (18.5 m^2) footprint. Remarkably, the laser acceleration region itself is less than 1 cm in length, with an acceleration gradient 10^4 times that of conventional linacs.[1,2] With the advent and continued development of such reliable, high-energy, narrow-band electron beams from compact (and potentially portable) sources, it becomes practical to now consider much more widespread application of energetic electron beams.

Electron beams approaching 1 GeV constitute a promising probe for non-destructive testing of critical components and active interrogation of concealed materials or structures. In this report, we focus in particular on concealed special nuclear material (SNM) at large standoff distances; Bremsstrahlung-based interrogations, as well as neutron beams, have typically been the focus for such applications at short range.[3,4,5] At energies approaching 1 GeV, electron ranges surpass the peak mean free path achievable for photons (areal density about 25 g cm^{-2}, occurring at x-ray energies ~10 MeV). A 500 MeV electron, for example, has a range of 6 cm (42 g cm^{-2}) in iron and 624 m in air. (Electron range characterizes the average distance over which all electron energy is lost, so somewhat smaller thicknesses or higher electron energies must be employed to maintain reasonable beam energy after transmission.) The range of 10 MeV electrons (as produced by a small conventional LINAC) is significantly smaller: 0.8 cm in iron and 43m in air – not usable for large standoff (tens of meters) nor for thick targets. Along with the highly penetrating nature of high-energy electrons, the narrow laser-accelerated beam provides high efficiency delivery to a distant target. Relative to Bremsstrahlung from a 10 MeV electron beam, which yields a 30° cone of radiation at intensity greater than 10% of its peak intensity,[6] our 6mrad beam would provide over 1000 times more efficient delivery at distance, while still illuminating a reasonable sub-meter-sized area at 100m. Very little bulky shielding or lead collimation would be required. Unlike x-rays,

electrons can be magnetically deflected, allowing an electron beam to be manipulated, redirected, or focused either before or after target interaction.

Our goal is to investigate the fundamental and practical limits of the use of an energetic beam from a laser accelerator for detection of SNM, under two main operational scenarios. First, radiography: a wakefield-accelerated electron beam is generated in the direction of a downstream target, e.g. cargo container at >10 m. As electrons traverse air or solid material, they will lose energy, primarily via Bremsstrahlung radiation as they are slightly deflected in interactions with electrons in the medium. Electrons that penetrate dense material will undergo more interactions than those that pass through air or low-density material; the result is a significant variation in electron energy and angular spread, corresponding to total areal density traversed. Imaging detectors downstream from the target will measure 2-D variations in deposited beam dose, with a dose deficit corresponding to high areal densities.[7]

Radiography using a laser-generated electron or X-ray beam can be extended to multiple dimensions or orientations with much less cost and effort than for a LINAC-based beam. A single pulsed laser can be split along multiple paths, each of which generates its own electron beam. Alternatively, fast switching optics can be employed to vary the laser path to produce different beam orientations for each pulse. Radiographs taken along different axes can be used to triangulate the 3-D location of dense items, or to enable the use of computed tomography to reconstruct the 3-D density structure of the target.

The second interrogation scenario we are investigating is nuclear activation. Activation using laser-accelerated electron beams is similar to LINAC-based activation, but leverages the large-standoff capability afforded by a high-energy electron beam. In this scenario, the electron beam is directed toward a target of interest; Bremsstrahlung x-rays produced by the electrons cause photonuclear reactions within the irradiated materials. The high efficiency of Bremsstrahlung conversion in heavy elements, and narrow angular divergence of high-energy Bremsstrahlung,[6] make SNM effectively self-intensifying. At these high energies, several photonuclear reactions are possible such as (γ, xn), (γ, p) and (γ, fission). The most interesting reaction is photofission. Prompt or delayed gamma-rays, or delayed neutron emissions, may be monitored as indicators of the parent isotopes present. The presence and intensity of particular delayed gamma energies, for example, could be monitored for traces of enriched SNM. Gammas will be particularly useful, as (1) prompt neutrons will be abundant from many materials given the high electron beam energies, and will likely

not be useful in distinguishing fissionable material; and (2) it may be challenging to distinguish e.g. ^{238}U from ^{235}U based on delayed neutron production, although more experimental work is required at these energies to better understand the utility of delayed neutrons produced by such high-energy beams.

Laboratory studies of activation and electron radiography have been carried out at the Diocles laser facility at the University of Nebraska. Monte Carlo simulations of electron beam transport over large distances (up to 100m) and through target materials and containers have also been performed. Our laboratory measurements, at meter-scale standoff, represent a significant advance over previous cm-scale experiments. The long range detection component of large standoff interrogation is not the focus of the present study; we restrict our investigation to: source capabilities; electron transport in air and resulting beam characteristics; interactions with containers/vessels, shielding, SNM, and additional overburden; and signal escape from the target vessel or container. We next describe the results of these experiments and models, and address advantages, challenges, and potential strategies for long-standoff interrogation using laser-accelerated high-energy electron beams.

ELECTRON BEAM PRODUCTION AND CHARACTERISTICS

Electron acceleration is achieved by focusing a high-intensity laser pulse into the gas jet injected from a supersonic nozzle into a 1.6 x 1.2 m vacuum chamber. Table 1 details the laser parameters used and the electron beam characteristics achieved. The electron beam can be passed through the gap of a moveable permanent magnet assembly, within the vacuum chamber, for deflection of the beam and energy spectrum determination. When undeflected, the beam passes through a 0.6 cm glass exit window into the room.

RADIOGRAPHY

After exiting the vacuum chamber and traveling the desired distance in the room (limited by the room size to about 5m), the electron beam can be imaged on storage phosphor image plates and read out using an image plate scanner. Radiography of solid targets is performed by interposing an object between window and image plate, optionally with one or more metal plates or blocks in place as shielding. Figure 1 shows a **single-shot** electron beam radiograph of a stainless steel rod with cross sectional shape of a capital letter "N," after beam transmission through 58 cm vacuum,

the chamber window, 24 cm air, and a 2.5 cm Al plate. The N-rod has dimensions 0.5 x 0.5 inches (1.27 x 1.27 cm) on the face and 1.0 inch (2.54 cm) depth, and was placed directly after the Al plate; the image plate was 6 cm downstream from the illuminated face of the N-rod. The electron beam energy was roughly 250 MeV. Planned radiography measurements include extension to higher beam energies, greater standoff distances, and a simulated cargo container arrangement.

Table 1. Parameters of electron beams and Diocles laser accelerator.

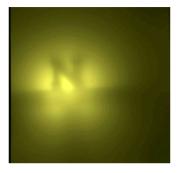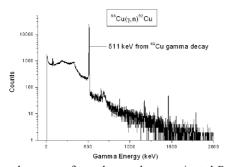|	
Laser power	3-80 TW
Central wavelength	805 nm
Pulse duration	30-60 fs
Nanosecond contrast	3×10^{-7}-2×10^{-8} cm^{-3}
Pulse energy	3.5 J
Pointing stability	3.5 mrad (1 min)
Laser intensity	1×10^{18}-3×10^{19} W cm^{-2}
Focal spot size	16 microns
Media	He, N$_2$
Plasma density	2×10^{18}-2×10^{19} cm^{-3}
Acceleration length	1, 2, 3 and 4 mm
Total electron beam charge	10 nC
High-energy component charge	0.1 nC

FIGURE 1. Single-shot electron beam radiograph of a 1.27x1.27x3.8 cm deep stainless steel N-bar, shielded by 2.5 cm Al. The illuminated face of the N-bar distance was located 84 cm from beam source and 6 cm from image plate. Millimeter-scale features are clearly apparent. (The platform and stalk supporting the N-bar are also visible.)

NUCLEAR ACTIVATION

Activation measurements were performed on copper targets, focusing on the ^{63}Cu(γ,n)^{62}Cu reaction. The primary experiment utilized 5.5 x 3.7 x 0.97 cm copper target of natural isotopic abundance. In order to intensify the Bremsstrahlung illumination of the Cu target, and to mimic a significant overburden of shielding or container walls, we attached a similarly-sized 0.78 cm thick Ta converter directly to the illuminated face of the Cu target. We placed the Ta+Cu target in the direct beam path, 70 cm from the electron beam source location, and fired 60 electron beam pulses (every 15 seconds) over 15 minutes. After the last shot, the Cu target (without Ta converter) was removed to a lead-shielded counting station and placed 9mm from the front face of a 45% efficient Ortec GEM coaxial germanium detector (83mm endcap diameter). Spectra were collected, then acquisition was halted, spectra recorded, and acquisition resumed at intervals (with roughly 10 second delays), for a total of about 1 hour (roughly 6 half-lives). The counts for each period within the 511 keV gamma peak were tallied, and start and stop times recorded. The result was the spectrum shown in Figure 2 including significant detectable 511 keV gamma radiation, exhibiting the expected 9.7-minute half-life decay of ^{62}Cu. Preliminary calculations indicate roughly 10^5 activations (^{62}Cu nuclei produced) per electron beam shot. We also performed activation of a Cu plate at 2 m from the beam source, crudely mimicking the arrangement of a target inside a steel cargo container: a similar Cu target was placed directly behind a 0.25 inch (0.64cm) thick stainless steel plate for electron beam illumination, and the activated copper spectrum was tallied through an identical stainless steel plate. Activation was substantial even in this less-intensified, shielded-detection arrangement. While these measurements are not the first cases of fully-laser-driven nuclear activation,[8,9] they were performed at significantly greater standoff than previous similar experiments.
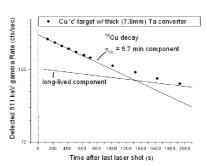

FIGURE 2. Measured spectrum from electron-beam-activated Cu target (left), and measured decay curve (right) exhibiting 9.7-minute half-life that identifies 62Cu. This is the longest-standoff activation performed using a laser-based source. This test case demonstrates capabilities to be applied to shielded SNM.

MONTE CARLO MODELS OF ACTIVE INTERROGATION

In order to consider in detail the application of high-energy electron beams to large standoff arrangements and to realistic-sized vessels containing fissile material, we developed Monte Carlo models of specific arrangements of interest. First, we considered the problem of beam delivery over long range through air. A GEANT Monte Carlo simulation was performed to investigate the geometry shown in Figure 3, with a point source of 400 MeV electrons (cone angle 8 mrad) exiting a vacuum chamber at 67 cm from source, and reaching a tally plane at 100 m from source. The electron fluence (normalized to maximum) of the resulting shower is also shown. This result indicates that a significant fraction of the electrons are undeflected or only slightly deflected, providing a beam of FWHM 1 m – only slightly greater than the 0.8 m width of the unscattered beam.
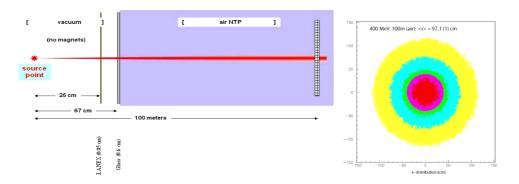

FIGURE 3. Simulation of 400 MeV electron transport through 100 m of air at STP. Left: geometry and material setup for radiography simulation. Right: GEANT Monte Carlo code calculation of normalized electron fluence at detection plane; contours indicate 0.17, 0.33, 0.5, 0.67, 0.83 of peak fluence. A large fraction of the beam remains undeflected or slightly deflected.

We also simulated electron transport through a 1.06 x 0.86 x 1.02 m wooden crate containing a 5 kg sphere of highly-enriched uranium using MCNPX. The crate was uniformly illuminated by 400 MeV electrons; the simulated geometry and the resulting electron fluence within the crate are shown in Figure 4. The electron fluence increases immediately after penetration into the crate, due to the production of lower-energy particle showers by the 400 MeV primary electrons. The U sphere casts a clear shadow downstream, through the remaining 0.5 m of the crate.
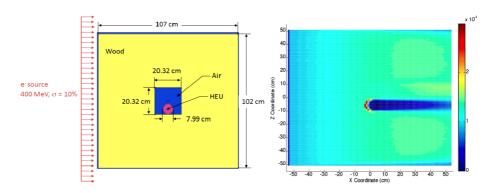

FIGURE 4. Simulation of 400 MeV electron transport and shower production in thick wooden crate containing highly enriched uranium (HEU). Left: simulated geometry; right, electron fluence (cm-2) throughout crate. Fluence grows after penetration into the crate, as incident electrons produce showers of lower-energy electrons. 8 cm HEU sphere casts a clear shadow through 0.5 m of wood.

DISCUSSION AND FUTURE WORK

It is clear that multiple small-angle electron scatterings pose an interesting challenge for high-resolution electron radiography; a tight correlation between detector location and path through target is required for good imaging, but scattering prior to, within, or after the target can deflect an interrogating electron. The magnification of such scattering by long travel enhances the blurring problem at long standoff distances. Magnetic focusing or physical collimation could potentially be used to selectively reject electrons after target interaction, eliminating those electrons whose angle relative to the known source location is too great. Time-of-flight variations could also provide a means for discriminating against highly deflected or greatly slowed electrons. Simulation studies of the evolution of energy and angular divergence of the electron beam in air and solids are required to make progress on this issue.

Activation is less sensitive to the effects of small-angle deflection, but (regardless of the penetrating power of the activating beam) activation measurements will be limited by the penetrating power of the measured secondary emissions. For any specific isotope to be monitored, selection of optimal emitted tracers will be critical. Identification of relatively high-energy gamma rays with significant production rates and appropriate decay times, and free from overlap with other lines, will be important. The spectral complexity of high-Z photofission products results in many lines to be investigated. Neutron measurement could be coupled with gamma-ray monitoring to help mitigate the effects of shielding.

The Diocles laser system will soon be upgraded to support 1 PW laser. We will use the increased power to generate higher-energy electron beams,up to 1 GeV. We also plan to increase the electron beam charge per bunch by the technique of optical injection.[10,11,12] These beam improvements will be applied to radiography and activation measurements through greater shielding and at distances up to 5 m from source. Increased repetition rate to 100 Hz is also targeted, and will provide improved capabilities for repeated pulsed interrogation modes.

SUMMARY

We have performed preliminary radiography and activation measurements using high-energy laser-accelerated electron beams in the laboratory. We have studied the transport of such beams over large distances in air and through shielded SNM. The low divergence and high penetration power of laser-accelerated high-energy electron beams, coupled with the compact source size, provide a compelling case for increased study of these beams as interrogation sources, particularly at large standoff distances.

ACKNOWLEDGEMENTS

REFERENCES

1. T. Tajima and J. Dawson, *Phys. Rev. Lett.* **43**, 267-270 (1979).
2. D. Umstadter, *Jour. Phys. D* **36**, R151–R165 (2003).
3. C.E. Moss, C.L. Hollas, G.W. Mckinney, and W.L. Myers, *IEEE Trans. Nuc. Sci.* **53**, 2242–2246 (2006).
4. G. Chen, G. Bennett, and D. Perticone, *Nucl. Instr. and Meth. B* **261**, (2007) 356.
5. M. Gmar et al., *Proc. SPIE* **6213**, 62130F (2006).
6. R.J. Faehl, C.M. Snell, and R.K. Keinigs, "Predicted Bremsstrahlung generation by energetic electron beams." Technical Report LA-11742-MS, Los Alamos National Laboratory, 1991.
7. S.P.D. Mangles et al., *Laser Part. Beams* **24**, 185-190 (2006).
8. S.A Reed et al., *Jour. Appl. Phys.* **102**, 073103–7 (2007).
9. W.P. Leemans, D. Rodgers, P.E. Catravas, C.G.R. Geddes, G. Fubiani, E. Esarey, B.A. Shadwick, R. Donahue, and A. Smith, *Phys. Plasmas* **8**, 2510–2516 (2001).
10. D. Umstadter, J. K. Kim, and E. Dodd, *Phys. Rev. Lett.* **76**, 2073-2076 (1996).
11. P. Zhang, N. Saleh, S. Chen, Z.M. Sheng, and D. Umstadter, *Phys. Rev. Lett.* **91**, 225001-1 (2003).
12. J. Faure, C. Rechatin, A. Norlin, A. Lifschitz, Y. Glinec, and V. Malka, *Nature* **444**, 737-739 (2006).